Optimization of Bipolar Toeplitz Measurement Matrix Based on Cosine-Exponential Chaotic Map and Improved Abolghasemi Algorithm

Shuo MENG [1], Chen MENG [1], Cheng WANG [1], Qiang WANG [2]

[1] Peoples Liberation Army Engineering University – Shijiazhuang, Shijiazhuang 050000, China
[2] Chemical Defence Institute, Beijing 102205, China

864748906@qq.com, 2895104899@qq.com, mengchen630101@163.com, 206407924@qq.com

Submitted May 17, 2023 / Accepted September 12, 2023 / Online first November 6, 2023

Abstract. *In compressive sensing theory, the measurement matrix plays a crucial role in compressive observation of sparse signals. The bipolar Toeplitz measurement matrix constructed based on chaotic map has advantages such as generating fewer free elements and supporting fast algorithms, making it widely used. While optimizing the measurement matrix can effectively improve its compressive sensing reconstruction performance, existing optimization algorithms are not suitable for the bipolar Toeplitz measurement matrix due to its structural and bipolar properties. To address this issue, this paper proposes an optimization method for the bipolar Toeplitz measurement matrix based on cosine-exponential (CE) chaotic map sequences and an improved Abolghasemi algorithm. Using an enhanced CE chaotic map to generate chaotic sequences with greater chaos and randomness, we construct the measurement matrix and optimize it using the structure matrix and the improved Abolghasemi algorithm, which preserves the matrix's bipolarity without altering its structure. We also introduce constraints on the generated sequence values during the optimization process. Through simulation experiments, the effectiveness of our optimization algorithm is verified, as the optimized bipolar Toeplitz measurement matrix significantly reduces reconstruction error and improves reconstruction probability.*

Keywords

Chaotic map, measurement matrix, bipolar Toeplitz matrix, optimization

1. Introduction

In 2006, Candes et al. discovered that if a signal has a good sparse representation, then the signal can be accurately reconstructed from its small number of non-adaptive linear measurements [1–6]. This led to the emergence of the new concept of "compressive sensing". Compressive sensing theory is able to accurately reconstruct high-dimensional signals with good sparse representations from a small number of non-adaptive linear measurements, which breaks the limitations of the Nyquist sampling theorem on the sampling process. It enriches the method of signal sampling theory and is widely used in fields such as broadband signal acquisition [7], medical imaging [8], and data compression [9], with great development prospects.

Compressive sensing theory consists of three parts: sparse representation, measurement matrix, and reconstruction algorithm [10]. Among them, the measurement matrix projects high-dimensional sparse signals onto low-dimensional space, playing a crucial role in compressive observation of sparse signals. The compression observation performance of the measurement matrix is usually measured by the restricted isometry property (RIP) [11], [12] and cross-correlation coefficients [13]. The better the compression observation performance, the higher the accuracy of signal reconstruction. When constructing the measurement matrix, RIP must be satisfied to obtain accurate measurement values of the original signal through a certain number of observations. For a measurement matrix that already satisfies RIP, the smaller the inter-correlation coefficient between the measurement matrix elements, the better the compression observation performance. Optimization algorithms are commonly used to reduce the correlation between the measurement matrix and the sparse dictionary or to enhance the independence among the measurement matrix column vectors, thereby reducing the cross-correlation coefficient.

The construction of the measurement matrix can generally be divided into random measurement matrices and deterministic measurement matrices according to the way in which the matrix elements are generated. The elements of a random measurement matrix are generated using a random sequence, ensuring that the matrix elements have high independence, so that random measurement matrices have good RIP and compression observation performance. However, too many free elements in a random measurement matrix are not conducive to hardware implementation [14], [15]. The elements of a deterministic measurement

DOI: 10.13164/re.2023.0583

matrix are generated using a deterministic function, and thus have repeatability and high hardware implementability. Deterministic measurement matrices constructed using chaotic sequences not only retain the advantages of random measurement matrices, but also have high hardware implementability, making them widely used. Popular chaotic maps include Logistic [16], Chebyshev [17], [18] and Cubic chaos [19], [20], etc.

In the process of constructing the measurement matrix, it is necessary to ensure that the matrix satisfies the Restricted Isometry Property (RIP) and that its elements are statistically approximately independent. Therefore, when constructing the measurement matrix using chaotic systems, it is common to sample the chaotic sequence with a relatively large sampling interval. This is because sampling intervals that are too close together can result in strong correlations among the elements of the measurement matrix, which can adversely affect its performance. In [21] and [22], measurement matrices were constructed based on the Logistic and Tent chaotic systems, respectively, with a minimum sampling interval of 15. However, this approach can lead to the generation of a large amount of redundant data during the sampling process, which wastes system resources. To address this problem, a polarized Toeplitz block measurement matrix based on bipolar chaotic sequences is proposed in [23]. By introducing bipolar functions to transform Chebyshev chaotic sequences into sequences consisting of −1 and +1, the sampling frequency of the measurement matrix elements is made equal to the frequency of sequence generation, reducing the sampling interval, increasing the utilization rate of elements, and avoiding resource waste.

However, chaotic mapping functions of Chebyshev, Logistic, and Cubic only enter into a chaotic state under specific conditions and produce chaotic sequences with low chaos density and weak randomness. This significantly affects the performance of the measurement matrix. Therefore, it is necessary to use some optimization algorithms to optimize the measurement matrix. However, some commonly used measurement matrix optimization algorithms, such as Elad algorithm [24], Duarte-Carvajalino algorithm [25], Abolghasemi algorithm [26], Gallagher algorithm [27], and singular value decomposition algorithm [28], when applied to the optimization of bipolar Toeplitz measurement matrices, will destroy the matrix structure and bipolarity.

From the above analysis, it can be seen that there are still some shortcomings in the construction and optimization of bipolar Toeplitz measurement matrices using existing methods, mainly including two aspects: first, the chaos density and randomness of chaotic map during the construction process will affect the compressive observation performance of the measurement matrix; second, traditional measurement matrix optimization algorithms will destroy the structure and bipolarity of bipolar Toeplitz measurement matrices.

To address these problems, this paper proposes a bipolar Toeplitz matrix optimization method based on the construction and optimization of the measurement matrix, using both the Cosine-exponential (CE) chaotic map and improved Abolghasemi algorithms. Firstly, the CE mapping is not limited by fractal coefficients and can quickly enter into a chaotic state with high chaos density and randomness, ensuring the performance of the constructed bipolar Toeplitz measurement matrix. Secondly, the structure matrix is introduced to represent the bipolar Toeplitz measurement matrix, and the improved Abolghasemi algorithm is used for optimization, which will not destroy the matrix structure and satisfies the constraint of threshold function, ensuring that the optimized matrix still has bipolarity. Experimental results show that the compressed sensing reconstruction error of the optimized bipolar Toeplitz measurement matrix is reduced, and the reconstruction probability is significantly improved.

The rest of this paper is organized as follows. In Sec. 2, we describe the expression of the CE chaotic sequence and analyze the method of constructing a bipolar Toeplitz measurement matrix using the CE chaotic sequence. In Sec. 3, we investigate the optimization method for bipolar Toeplitz measurement matrices. In Sec. 4, we combine simulation experiments to analyze the effectiveness of the constructed measurement matrix. Section 5 is the conclusion of the paper.

2. Description of the Problem

2.1 Chaotic Map

Chaotic systems are nonlinear systems with strong randomness. Since the expressions of chaotic systems are deterministic, their randomness is commonly referred to as "pseudo-randomness." Compared to random matrices, this "pseudo-random" characteristic guarantees the measurement matrix's performance while being easier to implement in hardware, striking a balance between the measurement matrix's performance and hardware implementation. Chaotic systems include low-dimensional and high-dimensional chaotic systems, with low-dimensional chaotic systems being widely used for their speed and efficiency. Typical one-dimensional chaotic maps such as Logistic, Cubic, and Chebyshev maps correspond to (1–3).

$$x_{j+1} = r x_j (1 - x_j), \quad x_j \in [-1,1], \tag{1}$$

$$x_{j+1} = \alpha x_j (1 - x_j^2), \quad x_j \in [0,1], \tag{2}$$

$$x_{j+1} = \cos(k \arccos(x_j)), \quad x_j \in [-1,1] \tag{3}$$

where r, α and k denote the fractal coefficients, i.e., the parameters of the chaotic state of the control system, and x_j and x_{j+1} denote the values of the chaotic map in the iterative process of the system.

When constructing measurement matrices using the aforementioned chaotic maps, there are some general drawbacks. First, the system can only enter chaos when the fractal coefficient exceeds a certain value. Second, the chaotic randomness of the three aforementioned mappings is poor, which is unfavorable for constructing measurement matrices. The stronger the randomness of the chaotic map, the smaller the correlation coefficient of the constructed measurement matrix, thereby yielding better compressive sensing performance. To address these issues, this paper introduces an enhanced CE chaotic sequence by incorporating exponential and polynomial functions based on the Logistic map.

$$x_{j+1} = \cos(\pi r x_j \, \mathrm{e}^{x_j}(1 + x_j) + 10\pi(\mathrm{e}^{x_j} + x_j^5)) \tag{4}$$

where the cosine function can control the function value in the interval of [−1,1], the introduction of the exponential term can break the restriction that the initial value is not zero, and $D = 10\pi(\exp x_j + x_j^5)$ can further enhance the chaotic density and randomness of the system. The bifurcation diagrams of the four chaotic systems corresponding to (1–4) are shown in Fig. 1.

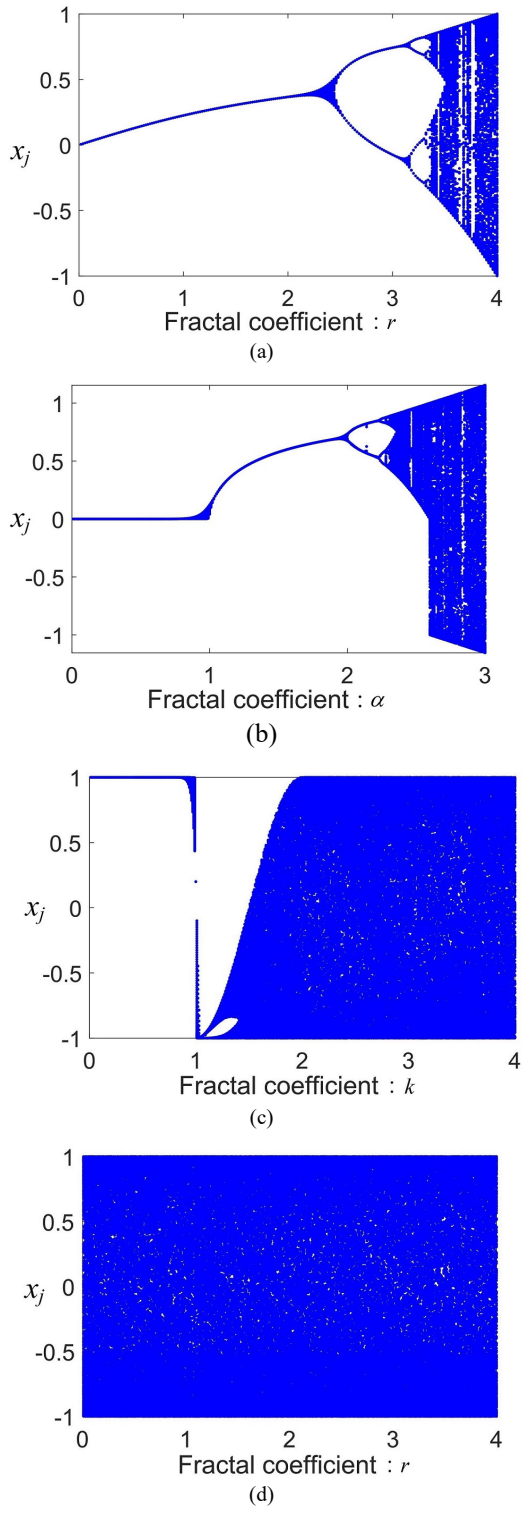

Fig. 1. Bifurcation diagrams of chaotic maps: (a) Logistic; (b) Cubic; (c) Chebyshev; (d) CE.

Figure 1 intuitively demonstrates that the CE chaotic system can quickly enter a chaotic state when the fractal coefficient is very small, and it outperforms the other three chaotic maps in Fig. 1.

Furthermore, analyzing the randomness and chaotic state of the chaotic map, the Lyapunov exponent (LE) is introduced as an evaluation index. The calculation formula for LE is defined as follows:

$$LE = \lim_{n\to\infty}\left(\frac{1}{n}\sum_{j=0}^{n-1}\ln\left|f'(x_j)\right|\right) \tag{5}$$

where $f'(x_j)$ represents the first-order derivative of the chaotic map $f(x_j) = x_{j+1}$. When $LE > 0$, the system is in a chaotic state, and the larger the LE value, the stronger the randomness of the chaotic sequence generated by the system. The relationship between the LE values of the four chaotic maps with respect to changes in fractal indices is shown in Fig. 2.

According to the results shown in Fig. 2, the LE values of the Logistic, Cubic, and Chebyshev mappings are not always greater than zero. The Logistic mapping enters a chaotic state when the fractal coefficient r is greater than 3.57; the Cubic mapping enters a chaotic state when the fractal coefficient α is greater than 2.3; and the Chebyshev mapping enters a chaotic state when the fractal coefficient k is greater than 2. On the other hand, the CE mapping can

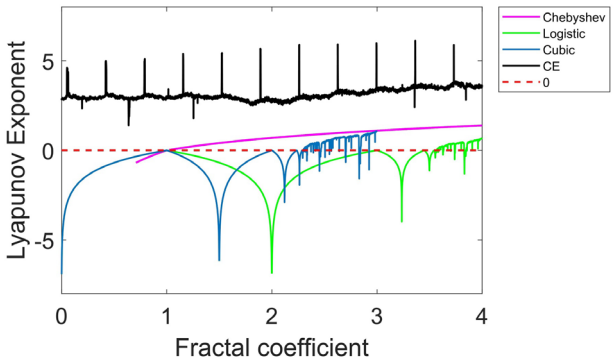

Fig. 2. Lyapunov exponent of different chaotic maps.

enter a chaotic state when the fractal coefficient is 0, and its LE value is always greater than zero and greater than that of the other three mappings. This indicates that the chaotic sequence generated by the CE mapping has stronger randomness.

2.2 Bipolar Toeplitz Measurement Matrix

Based on the enhanced CE chaotic sequence, a bipolar threshold function is introduced:

$$a_j = T(x_j) = \begin{cases} +1, & 0 \le x_j \le 1, \\ -1, & -1 \le x_j < 0. \end{cases} \tag{6}$$

Then the sequence $\{a_j\}$ constitutes a set of bipolar chaotic sequences:

$$a_{j+1} = \begin{cases} +1, & p = 0.5, \\ -1, & p = 0.5. \end{cases} \tag{7}$$

The enhanced bipolar chaotic sequence is used to construct the Toeplitz measurement matrix $\mathbf{\Phi} \in \mathbb{R}^{M \times N}$ with the following expression:

$$\mathbf{\Phi} = \frac{1}{\sqrt{M}} \begin{pmatrix} a_N & a_{N-1} & \cdots & a_2 & a_1 \\ a_{N+1} & a_N & \cdots & a_3 & a_2 \\ \vdots & \vdots & \ddots & \vdots & \vdots \\ a_{M+N-1} & a_{M+N-2} & \cdots & a_{M+1} & a_M \end{pmatrix} \tag{8}$$

where $\frac{1}{\sqrt{M}}$ is the column normalization factor.

According to the special structural characteristics of Toeplitz matrices, the measurement matrix $\mathbf{\Phi}$ can be divided into b Toeplitz matrices:

$$\mathbf{\Phi} = \left[\mathbf{\Phi}^{(1)} \ \mathbf{\Phi}^{(2)} \cdots \mathbf{\Phi}^{(b)} \right] \tag{9}$$

where $\mathbf{\Phi}^{(i)} \in \mathbb{R}^{M \times n} (i = 1,2,\ldots,b)$, $n = N/b$ ($n \in \mathbb{N}$) and each matrix $\mathbf{\Phi}^{(i)}$ has the structural characteristics of a Toeplitz matrix, and its expression is as follows:

$$\mathbf{\Phi}^{(i)} = \frac{1}{\sqrt{M}} \begin{bmatrix} a_n^{(i)} & a_{n-1}^{(i)} & \cdots & a_2^{(i)} & a_1^{(i)} \\ a_{n+1}^{(i)} & a_n^{(i)} & \cdots & a_3^{(i)} & a_2^{(i)} \\ \vdots & \vdots & \ddots & \vdots & \vdots \\ a_{M+n-1}^{(i)} & a_{M+n-2}^{(i)} & \cdots & a_{M+1}^{(i)} & a_M^{(i)} \end{bmatrix}. \tag{10}$$

Although the RIP of bipolar Toeplitz matrices have been effectively demonstrated in [11], the independence of the column vectors of the measurement matrix itself, as well as the correlation between the measurement matrix and the sparse dictionary, can both affect the compressive observation performance in practical applications. Therefore, it is necessary to further optimize the constructed Toeplitz matrix to ensure its effectiveness in practical applications. However, conventional measurement matrix optimization methods achieve this by reducing the numerical values of non-diagonal elements in the Gram matrix through techniques such as thresholding, gradient descent, or singular value decomposition. For Toeplitz matrices, using these optimization methods could destroy their structural and bipolar properties, making them unsuitable for optimizing bipolar Toeplitz measurement matrices. To address this issue, this paper proposes an improved Abolghasemi algorithm for bipolar Toeplitz measurement matrices.

3. Optimization of Bipolar Toeplitz Measurement Matrix

The fundamental principle of improving the Abolghasemi algorithm is to enhance the independence between column vectors of the bipolar Toeplitz measurement matrix or reduce the correlation between the measurement matrix and the sparse dictionary. This principle can be realized by lowering the Gram coefficient of the measurement or sensing matrix, after which the optimization objective function can be established.

3.1 The Optimization Objective Function

For a signal $\boldsymbol{x} \in \mathbb{R}^N$, the compressive sensing process can be represented as follows:

$$\boldsymbol{y} = \mathbf{\Phi}\boldsymbol{x} = \mathbf{\Phi}\mathbf{\Psi}\boldsymbol{s} \tag{11}$$

where $\boldsymbol{y} \in \mathbb{R}^M$ is the measurement data, $\mathbf{\Phi} \in \mathbb{R}^{M \times N}$ is the measurement matrix, $\mathbf{\Psi} \in \mathbb{R}^{N \times N}$ is the sparse dictionary, and $\boldsymbol{s} \in \mathbb{R}^N$ is the sparse vector.

Reducing the correlation between the measurement matrix and the sparse dictionary can effectively improve the compressive sensing reconstruction performance of compressed sampling system and the recovery accuracy of signals. The Gram matrix is defined as follows:

$$\mathbf{G} = \mathbf{\Psi}^{\mathrm{T}}\mathbf{\Phi}^{\mathrm{T}}\mathbf{\Phi}\mathbf{\Psi}\,. \tag{12}$$

The objective function of the measurement matrix can be expressed as:

$$\min_{\mathbf{G},\mathbf{G}_{\text{ideal}}} \left\| \mathbf{G} - \mathbf{G}_{\text{ideal}} \right\|_F^2 \tag{13}$$

where $\mathbf{G}_{\text{ideal}}$ is the ideal target matrix, whose expression will be introduced in subsequent section.

To ensure that the structural properties of the measurement matrix are unchanged during the optimization process, the measurement matrix is decomposed based on the number of free elements:

$$\mathbf{\Phi} = \sum_{j=1}^{J} a_j \mathbf{\Phi}^j \tag{14}$$

where $J = M + N - 1$ represents the number of free elements used to construct the Toeplitz matrix. The structural matrix corresponding to element a_j is denoted by $\mathbf{\Phi}^j$. $\mathbf{\Phi}^j$ has the same matrix dimension as $\mathbf{\Phi}$ and consists of two elements, 0 and $1/\sqrt{M}$. If the element at a given point in matrix $\mathbf{\Phi}^j$ is $1/\sqrt{M}$, the element at that position in matrix $\mathbf{\Phi}$ is a_j. So equation (11) can be expanded as follows:

$$\begin{aligned}\mathbf{\Phi} &= \begin{pmatrix} 0 & \cdots & a_1 \\ \vdots & \ddots & \vdots \\ 0 & \cdots & 0 \end{pmatrix} + \ldots + \begin{pmatrix} 0 & \cdots & 0 \\ \vdots & \ddots & \vdots \\ a_{M+N-1} & \cdots & 0 \end{pmatrix} \\ &= a_1\mathbf{\Phi}^1 + \ldots + a_{M+N-1}\mathbf{\Phi}^{M+N-1}.\end{aligned} \tag{15}$$

$\mathbf{\Phi}^j$ in (14) can be expressed as follows:

$$\mathbf{\Phi}^1 = \begin{pmatrix} 0 & \cdots & 1/\sqrt{M} \\ \vdots & \ddots & \vdots \\ 0 & \cdots & 0 \end{pmatrix}, \ldots, \mathbf{\Phi}^{M+N-1} = \begin{pmatrix} 0 & \cdots & 0 \\ \vdots & \ddots & \vdots \\ 1/\sqrt{M} & \cdots & 0 \end{pmatrix}. \tag{16}$$

Substituting (14) into (13), the optimization objective function of the measurement matrix can be expressed as:

$$\begin{aligned}&\min_{\{a_j\},\mathbf{G}_{\text{ideal}}} f(\{a_j\},\mathbf{G}_{\text{ideal}}) \\ &= \left\| \mathbf{\Psi}^{\mathrm{T}} \left(\sum_{j=1}^{J} a_j (\mathbf{\Phi}^j)^{\mathrm{T}}\right)\left(\sum_{j=1}^{J} a_j \mathbf{\Phi}^j\right)\mathbf{\Psi} - \mathbf{G}_{\text{ideal}} \right\|_F^2.\end{aligned} \tag{17}$$

To maintain the structural properties of the measurement matrix, only sequence $\{a_j\}$ needs to be optimized in the objective function optimization process.

3.2 Improved Abolghasemi Algorithm

The basic idea underlying the original Abolghasemi algorithm is to alternate between updating the Gram matrix and the measurement matrix $\mathbf{\Phi}$. However, optimizing $\mathbf{\Phi}$ directly would destroy its structural properties. Therefore, in this paper, optimization of the measurement matrix is achieved through updating the sequence $\{a_j\}$ while ensuring the structural properties of the measurement matrix.

First, the ideal Gram matrix $\mathbf{G}_{\text{ideal}}$ is updated using shrinkage operation:

$$\forall i,j,i \neq j, G\_\text{ideal}_{ij} = \begin{cases} g_{ij}, |g_{ij}| \leqslant \mu_{\text{welch}} \\ \mu_{\text{welch}} \cdot \text{sign}(g_{ij}), |g_{ij}| > \mu_{\text{welch}} \end{cases} \tag{18}$$

where G_ideal_{ij} is the element of the target matrix, sign(·) is the sign function, g_{ij} denotes the ij-th element of the $\mathbf{G} = \mathbf{\Psi}^{\mathrm{T}}\mathbf{\Phi}^{\mathrm{T}}\mathbf{\Phi}\mathbf{\Psi}$, μ_{welch} is mutual coherence lower bound (Welch bound), which is defined as follows:

$$\mu_{\text{Welch}} = \sqrt{\frac{M-N}{N(M-1)}} \tag{19}$$

where M and N are the size parameters of the measurement matrix.

Then, the elements in the sequence $\{a_j\}$ are updated using gradient descent algorithm:

$$a_j^{i+1} = a_j^i - \eta \frac{\partial}{\partial a_j^i} f(\{a_j\},\mathbf{G}_{\text{ideal}}) \tag{20}$$

where η is the step size of the gradient descent.

3.3 The Constraints on the Sequence $\{a_j\}$

Although the improved Abolghasemi algorithm can ensure that the structural properties of the measurement matrix remain unchanged, it cannot maintain the bipolarity of the measurement matrix. Therefore, this paper constrains the sequence $\{a_j\}$ during the iterative process using a threshold function:

$$a_j^{i+1} = \begin{cases} +1, & a_j^{i+1} \geq 0, \\ -1, & a_j^{i+1} < 0. \end{cases} \tag{21}$$

The bipolar threshold constraint function in (21) can preserve the bipolarity of the measurement matrix during the optimization process. When the iteration meets the termination condition, we obtain the optimized sequence and calculate the measurement matrix according to (14). The proposed optimization algorithm for the bipolar Toeplitz matrix is shown in Algorithm 1.

Algorithm 1: The optimization algorithm for bipolar Toeplitz measurement matrix

Input: Bipolar Toeplitz measurement matrix $\mathbf{\Phi}$, sparse dictionary $\mathbf{\Psi}$

Output: Optimized $\mathbf{\Phi}$

Step 1: Construct the sequence $\{a_j\}$ and structural matrix $\{\mathbf{\Phi}^j\}$ using the input measurement matrix $\mathbf{\Phi}$.

Step 2: Update $\mathbf{G}_{\text{ideal}}$ using (18).

Step 3: Update each element a_j in the sequence $\{a_j\}$ individually using (20).

Step 4: Apply (21) to constrain the modified elements a_j.

Step 5: Verify that the criterion for iteration termination has been met. If so, go to Step 6. If not, go back to Step 2.

Step 6: Using (14), output the optimized measurement matrix $\mathbf{\Phi}$.

4. Experiments and Analysis

To validate the effectiveness of the proposed method, numerical simulations are conducted to analyze the optimization effect of the measurement matrix and the compressive sensing reconstruction performance of the optimized matrix.

4.1 Performance Analysis of the Optimization Algorithm

Since the CE chaotic sequence proposed in this paper is an improvement based on the Logistic chaotic map,

a comparative experiment was conducted to construct a Logistic chaotic sequence using the following four methods:

1) $\mathbf{\Phi}_1$, a bipolar Toeplitz measurement matrix based on the Logistic chaotic map;
2) Optimized $\mathbf{\Phi}_1$;
3) $\mathbf{\Phi}_2$, a bipolar Toeplitz measurement matrix based on the CE chaotic map;
4) Optimized $\mathbf{\Phi}_2$.

The parameters of the measurement matrix are set as $N = 256$ and $M = 128$, and the optimization process of two different bipolar Toeplitz measurement matrices, $\mathbf{\Phi}_1$ and $\mathbf{\Phi}_2$, is shown in Fig. 3. As seen from Fig. 3, with an increased number of iterations, the objective function continuously decreases. And the objective function converges quickly after a smaller number of iterations, which is due to the structural properties of the bipolar Toeplitz matrix and the bipolar property that largely limits the optimization space of the measurement matrix.

To better assess the performance of four measurement matrices, introduce the average mutual coherence and maximum cross-correlation coefficient.

$$\mu_{\max} = \max_{1\le n,n'\le N, n\ne n'} \left|\mathbf{G}(n,n')\right|, \tag{22}$$

$$\mu_{\text{av}} = \frac{1}{N(N-1)} \sum_{1\le n,n'\le N, n\ne n'} \left|\mathbf{G}(n,n')\right|. \tag{23}$$

Table 1 shows the average and maximum normalized mutual correlation coefficients of four different measurement matrices. From Tab. 1, it can be seen that the proposed optimization algorithm is effective in reducing the coherence between the measurement matrix and the sparse dictionary. The average and maximum correlation coefficients are significantly reduced, and the proposed method's correlation coefficient is much smaller than that of the logistic construction measurement matrix. This is because the CE mapping can generate chaotic sequences with stronger randomness and chaos, thereby reducing the correlation between the constructed measurement matrix column vectors.

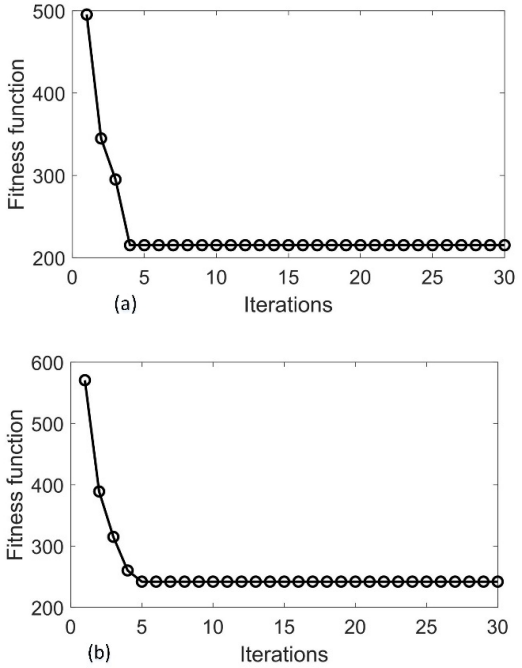

Fig. 3. Optimization of the bipolar Toeplitz measurement matrix. (a) The optimization of $\mathbf{\Phi}_1$; (b) The optimization of $\mathbf{\Phi}_2$.

Method	$\mu_{\max}$	μ_{av}
$\mathbf{\Phi}_1$	0.4975	0.0965
Optimized-$\mathbf{\Phi}_1$	0.3125	0.0719
$\mathbf{\Phi}_2$	0.3281	0.0675
Optimized-$\mathbf{\Phi}_2$	**0.2384**	**0.0629**

Tab. 1. Correlation coefficient.

4.2 Experimental Analysis of Linear Frequency Modulation (LFM) Signals

LFM signals are a typical non-stationary signals with advantages such as high target resolution, anti-interference, and strong anti-jamming capabilities, making them widely used in radar applications. Therefore, using LFM signals to verify the effectiveness of the proposed method has practical significance. The model expression of the LFM signal is defined as follows:

$$x(t) = \sum_{i=1}^{K} A_i \exp\left[\mathrm{j}2\pi\left(f_i t + \frac{1}{2}k_i t^2\right)\right] \tag{24}$$

where K is the number of LFM signal components, A_i and f_i are the amplitude and initial frequency of the i-th component respectively, and k_i is the chirp rate of the i-th component.

Although the LFM signal itself does not exhibit sparsity, considering that the LEM signal has good sparsity in the fractional Fourier transform (FRFT) domain, the FRFT dictionary is used as the sparse representation dictionary for the LFM signal in this paper. During the experiment, a four-component LFM signal was selected as the analysis object, and its parameters were set as shown in Tab. 2. The time-domain, frequency-domain, and sparse representation of the LFM signal are shown in Fig. 4. Figure 4 shows that the LFM signal has good sparsity in the fractional Fourier transform domain (FRFT-domain).

Parameter	Values
K	4
A_i	[0.9 1.1 1.1 0.9]
f_i (MHz)	[100 200 300 400]
k (MHz)	–300
T (μs)	1

Tab. 2. LFM signal parameters.

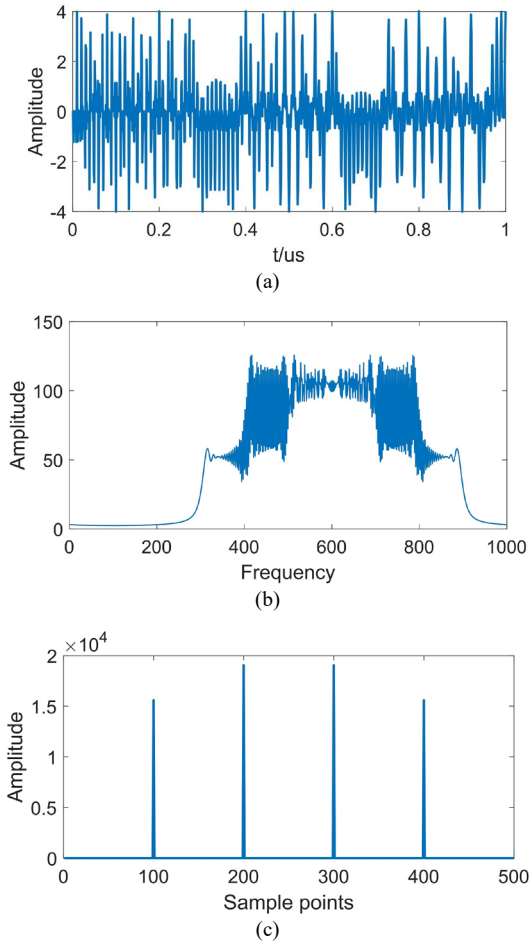

Fig. 4. LFM signal. (a) Time domain diagram; (b) Fourier transform; (c) FRFT-sparse representation.

As Fig. 4(c) exhibits the best sparsity representation effect, utilizing the proposed method to analyze Fig. 4(c) can result in higher reconstruction accuracy. During the experiment, four different measurement matrices were compared, with the measurement matrix parameters set as $N = 500$ and $M = 128$. The orthogonal matching pursuit (OMP) algorithm was used for reconstruction, and the reconstruction results of $\mathbf{\Phi}_1$ and optimized $\mathbf{\Phi}_1$ are shown in Fig. 5. The reconstruction results of $\mathbf{\Phi}_2$ and optimized $\mathbf{\Phi}_2$ are shown in Fig. 6.

From the reconstruction results, it can be seen that under the condition of $M = 128$, all four measurement matrices achieved effective reconstruction of the fractional

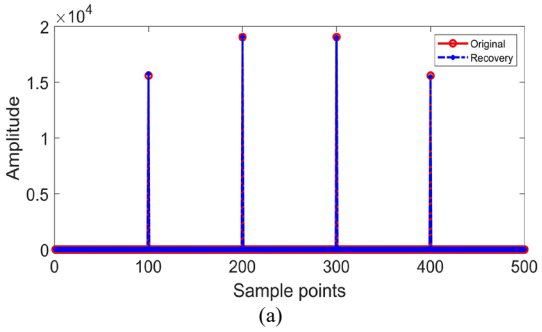

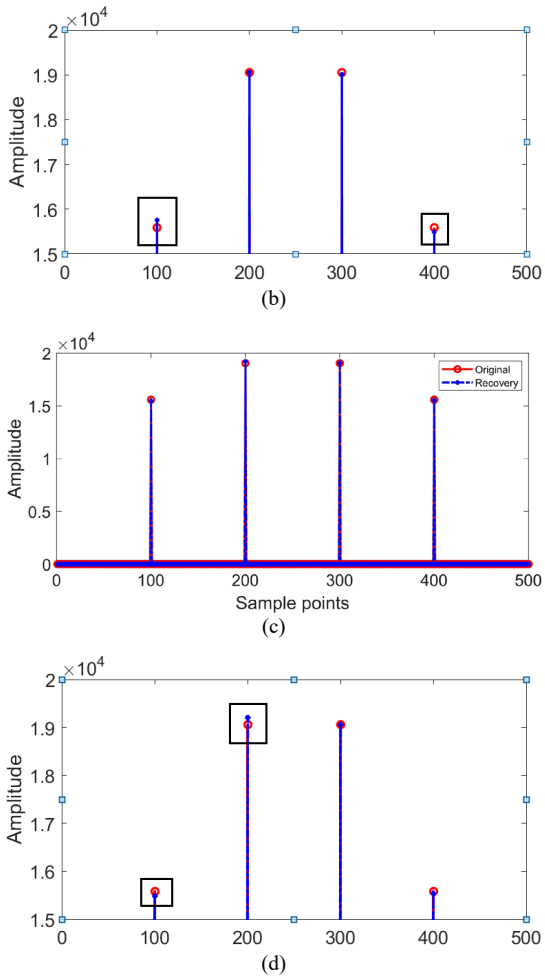

Fig. 5. Recovery results of the measurement matrix $\mathbf{\Phi}_1$. (a) $\mathbf{\Phi}_1$, recovery rendering; (b) $\mathbf{\Phi}_1$, detail drawing of recovery rendering; (c) Optimized $\mathbf{\Phi}_1$, recovery rendering; (d) Optimized $\mathbf{\Phi}_1$, detail drawing of recovery rendering.

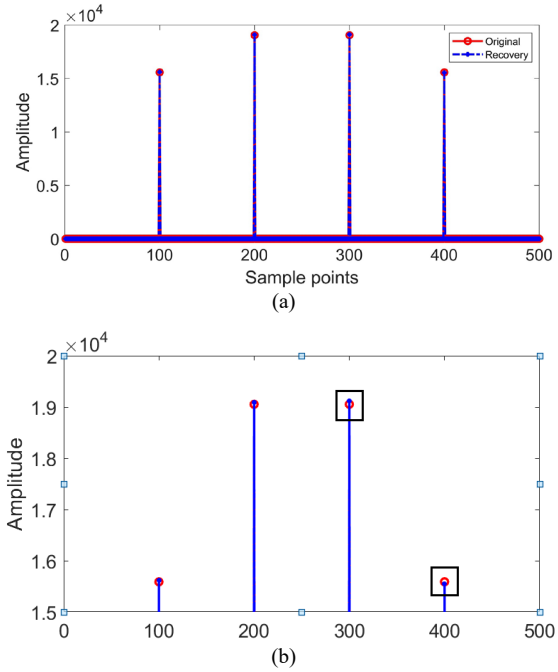

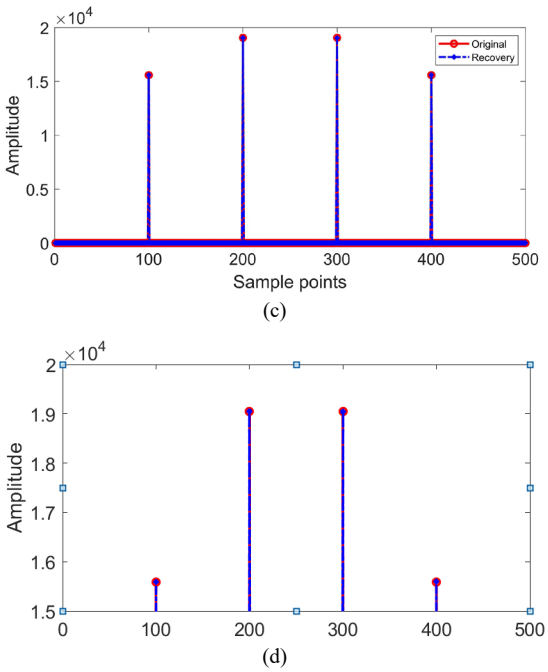

Fig. 6. Recovery results of the measurement matrix $\boldsymbol{\Phi}_2$. (a) $\boldsymbol{\Phi}_2$, recovery rendering; (b) $\boldsymbol{\Phi}_2$, detail drawing of recovery rendering; (c) Optimized $\boldsymbol{\Phi}_2$, recovery rendering; (d) Optimized $\boldsymbol{\Phi}_2$, detail drawing of recovery rendering.

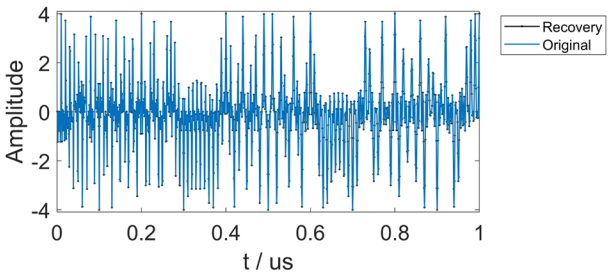

Fig. 7. Original and recovery LFM signal.

Fourier spectrum. However, a comparison of the reconstruction errors in the detail chart reveals that the reconstruction error of the optimized measurement matrix is significantly reduced, and the reconstruction performance of $\boldsymbol{\Phi}_2$ is better than that of $\boldsymbol{\Phi}_1$.

Combining the above analysis shows that using the proposed method to reconstruct the fractional Fourier spectrum can improve the reconstruction accuracy. In conjunction with the FRFT sparse representation dictionary and the sparse coefficient for signal recovery, the recovered signal is shown in Fig. 7. It can be seen from Fig. 7 that the reconstructed signal is almost identical to the original signal.

In practical applications, noise in the signal measurement process is inevitable. Therefore, different signal-to-noise ratios (SNR) of noise were added to the compression sampling process to analyze the reconstruction performance of the four measurement matrices under noisy conditions. During the experiment, the SNR was set to increase from 10 dB to 30 dB, and when the relative reconstruction error was less than 10^{-2}, it was considered as

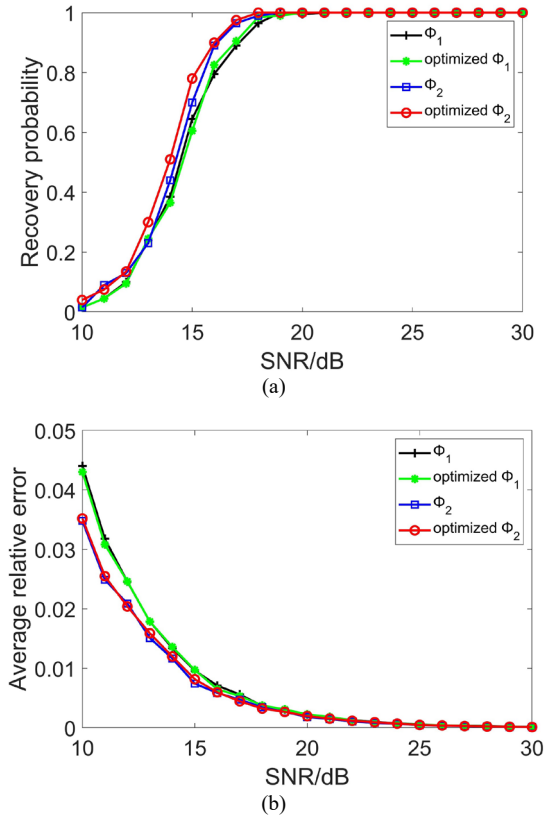

Fig. 8. Recovery performance with different SNRs: (a) Recovery probability; (b) Relative error in average.

successful; otherwise, it was a failure. The reconstruction success rate and average relative error of the four measurement matrices under different SNR conditions are shown in Fig. 8.

It can be observed from Fig. 8 that the performance of the optimized measurement matrix was improved. When SNR $\geq$ 19 dB, the performance of the four measurement matrices was comparable, with a reconstruction success rate approaching 1, and the average relative error was also very close. When SNR < 19 dB, it is evident from the figure that the reconstruction success rate of the measurement matrix constructed based on CE mapping approaches 1 faster, and the average relative error is significantly lower than other methods. Therefore, the proposed method is beneficial for improving the compressive sensing reconstruction performance under noisy conditions.

4.3 Experimental Analysis of Two-Dimensional Data

This paper further validates the proposed method using two-dimensional data. In the experiment, two classic image photos with a size of 256 × 256 were selected for analysis. Each image was divided into 256 blocks of size 16 × 16, and then compressed sensing reconstruction experiments were conducted. Since the image data used in this paper has certain sparsity in the wavelet transform domain, a discrete wavelet dictionary was used as the sparse dictionary in the experiment. The measurement

matrix was still compared using the four different schemes in Sec. 4.1, and the size of the observation matrix was set to 256 × 128. The original image and the reconstruction results of the two pictures are shown in Figs. 9 and 10, respectively, and it can be observed from the figures and the calculated relative reconstruction error that the performance of the two different optimized measurement matrices has been improved, and the proposed method has a better compression reconstruction effect.

Furthermore, to analyze the impact of the number of observations on the performance of the measurement matrix, the experiment set the number of observations to increase from 80 to 180 and obtained the reconstruction error results of the four different measurement matrices as shown in Fig. 11. From the experimental results shown in Fig. 11, it can be seen that the reconstruction error of the image decreases continuously with the increase of the number of observations. Although the performance of the four measurement matrices is not significantly different, the experimental results of the four different methods show that the performance of the measurement matrix corresponding to CE is always better than that of the Logistic-measurement matrix, and the optimization algorithm can further improve the performance of the measurement matrix.

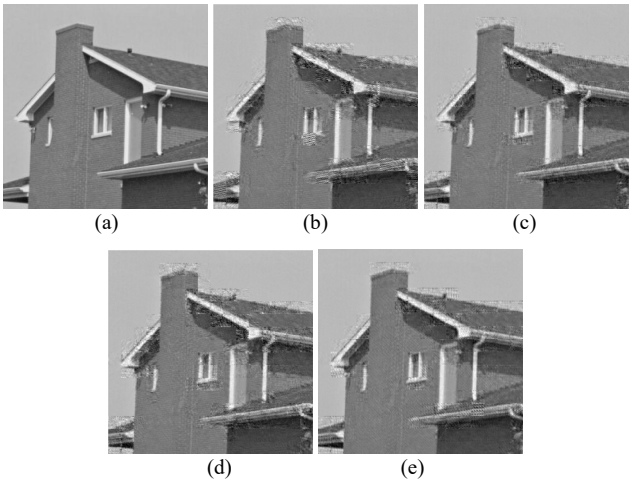

Fig. 9. "House" (a) Original image; (b) $\mathbf{\Phi}_1$, error = 4.8926×10^{-04}; (c) Optimized $\mathbf{\Phi}_1$, error = 3.2987×10^{-04}; (d) $\mathbf{\Phi}_2$, error = 3.9618×10^{-04}; (e) Optimized $\mathbf{\Phi}_2$, error = 2.7346×10^{-04}.

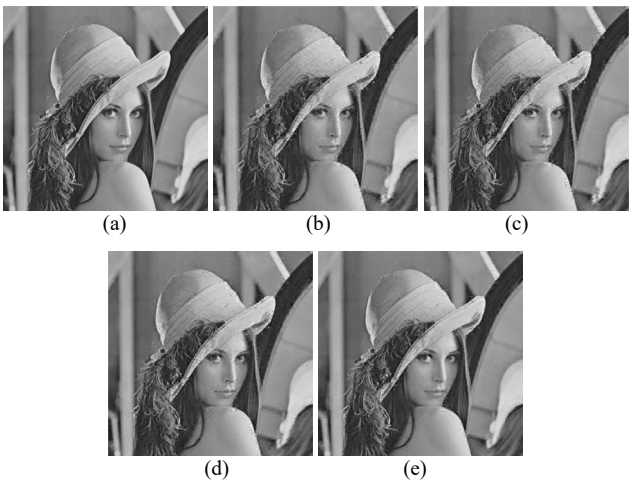

Fig. 10. "Lena" (a) Original image; (b) $\mathbf{\Phi}_1$, error = 2.1841×10^{-04}; (c) Optimized $\mathbf{\Phi}_1$, error = 1.6209×10^{-04}; (d) $\mathbf{\Phi}_2$, error = 1.3918×10^{-04}; (e) Optimized $\mathbf{\Phi}_2$, error = 9.3071×10^{-05}.

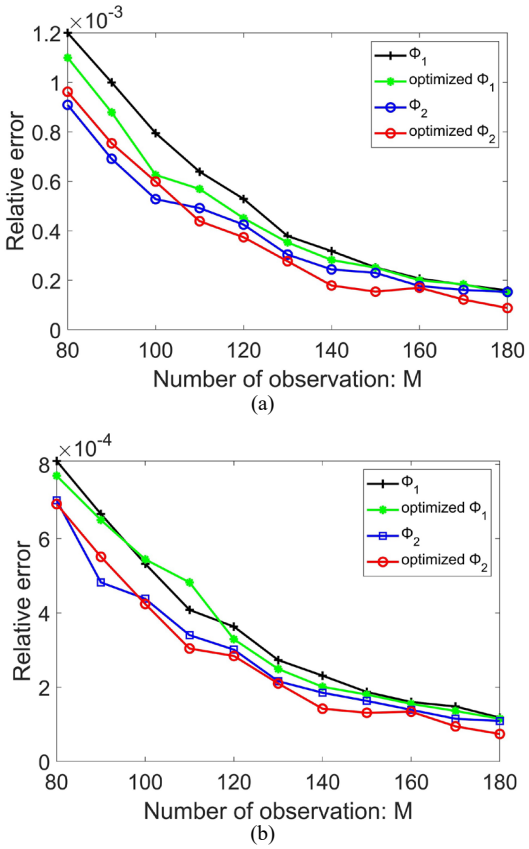

Fig. 11. Recovery error with different observations: (a) "House"; (b) "Lena".

4.4 Analysis of Different Reconstruction Algorithms

To further validate the effectiveness of the proposed methods in this paper and engage in a broader discussion, various reconstruction algorithms were employed in the reconstruction process:

(1) FISTA: Fast Iterative Shrinkage-Thresholding Algorithm ;

(2) ISTA: Iterative Shrinkage-Thresholding Algorithm ;

(3) OMP: Orthogonal Matching Pursuit ;

(4) CoSaMP: Compressive Sampling Matching Pursuit.

Using the aforementioned methods, the reconstruction of the LFM signals in Sec. 4.2 and the "House" image in Sec. 4.3 were performed. The reconstructions were considered successful when the relative reconstruction error was less than 10^{-2}. The success probability of the reconstruction for both signals can be seen in Fig. 12 and Fig. 13, respectively.

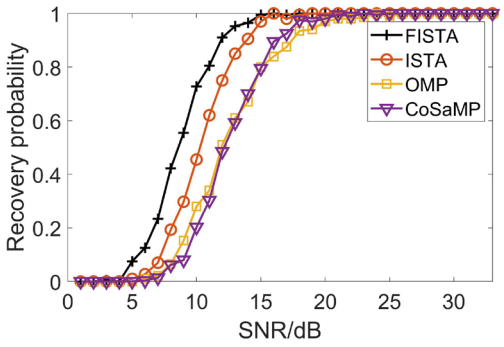

Fig. 12. LFM signals with different reconstruction algorithms.

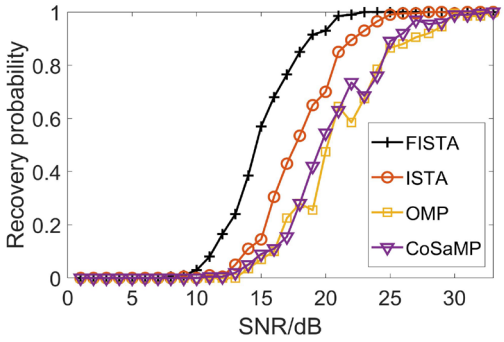

Fig. 13. "House" with different reconstruction algorithms.

The results depicted in the figures demonstrate that the proposed methods, in combination with different reconstruction algorithms, can achieve successful reconstruction of both one-dimensional and two-dimensional signals, maintaining a high reconstruction probability. Furthermore, based on the reconstruction results shown in the figures, there is little difference in performance among different reconstruction algorithms, indicating the adaptability of the proposed methods to various reconstruction algorithms.

5. Conclusion

This paper proposes a novel optimization method for bipolar Toeplitz matrices, which enhances the measurement matrix performance in two aspects. Firstly, a CE mapping is proposed, and the constructed measurement matrix with enhanced CE mapping has better compressive observation performance. Secondly, by introducing structural matrices, improving the Abolghasemi optimization algorithm, and constraining the threshold function, the structural characteristics and bipolarity of the Toeplitz matrix are ensured during the optimization process. Experimental results show that the proposed method not only reduces the correlation coefficient of the measurement matrix but also effectively applies to the compressive sensing reconstruction of one-dimensional signals and two-dimensional images when combined with sparse representation dictionaries. Compared with the previous methods, the reconstruction error is significantly reduced, and the reconstruction performance is significantly improved.

Acknowledgments

This work is supported by the National Natural Science Foundation of China (Grant No. 61501493).

References

[1] CANDES, E. J. Compressive sampling. In *International Congress of Mathematicians*. Madrid (Spain), 2007. Vol. III (Invited Lectures), p. 1433–1452. DOI: 10.4171/022-3/69

[2] CANDES, E. J., ROMBERG, J. Quantitative robust uncertainty principles and optimally sparse decompositions. *Foundations of Computational Mathematics*, 2006, vol. 6, p. 227–254. DOI: 10.1007/s10208-004-0162-x

[3] CANDES, E. J., ROMBERG, J., TAO, T. Robust uncertainty principles: Exact signal reconstruction from highly incomplete frequency information. *IEEE Transactions on Information Theory*, 2006, vol. 52, no. 2, p. 489–509. DOI: 10.1109/TIT.2005.862083

[4] CANDES, E. J., ROMBERG, J., TAO, T. Stable signal recovery from incomplete and inaccurate measurements. *Communications on Pure and Applied Mathematics,* 2006, vol. 59, no. 8, p. 1207 to 1223. DOI: 10.1002/cpa.20124

[5] CANDES, E. J., TAO, T. Near-optimal signal recovery from random projections: Universal encoding strategies. *IEEE Transactions on Information Theory*, 2006, vol. 52, no. 12, p. 5406–5425. DOI: 10.1109/TIT.2006.885507

[6] DONOHO, D. L. Compressed sensing. *IEEE Transactions on Information Theory*, 2006, vol. 52, no. 4, p. 1289–1306. DOI: 10.1109/TIT.2006.871582

[7] AJAMIAN, T., MOUSSAOUI, S., DUPRET, A., et al. Compressed signal acquisition in wire diagnostic. In *IEEE Sensors*. Glasgow (UK), 2017, p. 1–3. DOI: 10.1109/ICSENS.2017.8234017

[8] AMBROSANIO, M., KOSMAS, P., PASCAZIO, V. A multi-threshold iterative DBIM-based algorithm for the imaging of heterogeneous breast tissues. *IEEE Transactions on Biomedical Engineering*, 2019, vol. 66, no. 2, p. 509–520. DOI: 10.1109/TBME.2018.2849648

[9] WANG, Q., MENG, C., WANG, C. Compressive sampling and reconstruction for LFM signals with unknown modulating rate based on Gabor space (in Chinese). *Journal of Signal Processing*, 2022, vol. 38, no. 4, p. 747–758. DOI: 10.16798/j.issn.1003-0530.2022.04.009

[10] CANDES, E. J., TAO, T. Decoding by linear programming. *IEEE Transactions on Information Theory*, 2005, vol. 51, no. 12, p. 4203-4215. DOI: 10.1109/TIT.2005.858979

[11] BARANIUK, R., DAVENPORT, M., DEVORE, R., et al. A simple proof of the restricted isometry property for random matrices. *Constructive Approximation*, 2008, vol. 28, no. 3, p. 253–263. DOI: 10.1007/s00365-007-9003-x

[12] BAI, H., LI, G., LI, S., et al. Alternating optimization of sensing matrix and sparsifying dictionary for compressed sensing. *IEEE Transactions on Signal Processing*, 2015, vol. 63, no. 6, p. 1581–1594. DOI: 10.1109/TSP.2015.2399864

[13] CHEN, Y. J., ZHANG, Q., LUO, Y., et al. Measurement matrix optimization for ISAR sparse imaging based on genetic algorithm. *IEEE Geoscience and Remote Sensing Letters*, 2016, vol. 13, no. 12, p. 1875–1879. DOI: 10.1109/LGRS.2016.2616352

[14] RAGHEB, T., LASKA, J. N., NEJATI, H., et al. A prototype hardware for random demodulation based compressive analog-to-

digital conversion. In *2008 51st Midwest Symposium on Circuits and Systems*. Knoxville (TN, USA), 2008, p. 37–40. DOI:10.1109/MWSCAS.2008.4616730

[15] ARIE, R., BRAND, A., ENGELBERG, S. Compressive sensing and sub-Nyquist sampling. *IEEE Instrumentation and Measurement Magazine*, 2020, vol. 23, no. 2, p. 94–101. DOI: 10.1109/MIM.2020.9062696

[16] YU, L., BARBOT, J. P., ZHENG, G., et al. Compressive sensing with chaotic sequence. *IEEE Signal Processing Letters*, 2010, vol. 17, no. 8, p. 731–734. DOI: 10.1109/LSP.2010.2052243

[17] YI, R., CUI, C., MIAO, Y., et al. A method of constructing measurement matrix for compressed sensing by Chebyshev chaotic sequence. *Entropy*, 2020, vol. 22, no. 10, p. 1–16. DOI: 10.3390/e22101085

[18] BENAZZOUZA, S., RIDOUANI, M., SALAHDINE, F., et al. Chaotic compressive spectrum sensing based on Chebyshev map for cognitive radio networks. *Symmetry*, 2021, vol. 13, p. 1–22. DOI: 10.3390/sym13030429

[19] ZHANG, Y. The unified image encryption algorithm based on chaos and cubic S-Box. *Information Sciences*, 2018, vol. 450, p. 361–377. DOI: 10.1016/j.ins.2018.03.055

[20] KAMEL, S. H., ABD-EL-MALEK, M. B., EL-KHAMY, S. E. Compressive spectrum sensing using chaotic matrices for cognitive radio networks. *International Journal of Communication Systems*, 2019, vol. 32, no. 6, p. 1–16. DOI: 10.1002/dac.3899

[21] VLAD, A., LUCA, A., FRUNZETE, M. Computational measurements of the transient time and of the sampling distance that enables statistical independence in the logistic map. In *International Conference on Computational Science and Its Applications (ICCSA 2009)*. Seoul (Korea), 2009, vol. 2, p. 703 to 718. DOI: 10.1007/978-3-642-02457-3_59

[22] VADUVA, A., VLAD, A., BADEA, B. Evaluating the performance of a test-method for statistical independence decision in the context of chaotic signals. In *2016 International Conference on Communications (COMM).* Bucharest (Romania), 2016, p. 417 to 422. DOI: 10.1109/ICComm.2016.7528207

[23] GAN, H., ZHANG, T., HUA, Y., et al. Toeplitz-block sensing matrix based on bipolar chaotic sequence (in Chinese). *Acta Physica Sinica -Chinese Edition*, 2021, vol. 70, no. 3, p. 1–12.

[24] ELAD, M. Optimized projections for compressed sensing. *IEEE Transactions on Signal Processing*, 2007, vol. 55, no. 12, p. 5695 to 5702. DOI: 10.1109/TSP.2007.900760

[25] DUARTE-CARVAJALINO, J. M., SAPIRO, G. Learning to sense sparse signals: Simultaneous sensing matrix and sparsifying dictionary optimization. *IEEE Transactions on Image Processing*, 2009, vol. 18, no. 7, p. 1395–1408. DOI: 10.1109/TIP.2009.2022459

[26] ABOLGHASEMI, V., FERDOWSI, S., SANEI, S. A gradient-based alternating minimization approach for optimization of the measurement matrix in compressive sensing. *Signal Processing*, 2012, vol. 92, no. 4, p. 999–1009. DOI: 10.1016/j.sigpro.2011.10.012

[27] WICKER, S. B., KIM, S. Low-density parity-check codes. In *Fundamentals of Codes, Graphs, and Iterative Decoding. The International Series in Engineering and Computer Science*, vol. 714, ch. 8, p. 137–175. DOI: 10.1007/0-306-47794-7_8

[28] ATIF, S. M., QAZI, S., GILLIS, N. Improved SVD-based initialization for nonnegative matrix factorization using low-rank correction. *Pattern Recognition Letters*, 2019, vol. 122, p. 53–59. DOI: 10.1016/j.patrec.2019.02.018

About the Authors ...

Shuo MENG was born in 1996. He received the M.S. degree from the Army Engineering University of PLA–Shijiazhuang, Shijiazhuang, China, in 2020, where he is currently pursuing the Ph.D. degree. His current research interests include compressive sensing, analog to information conversion and signal processing.

Chen MENG (corresponding author) was born in 1963, he received the Ph.D. degree from the Nanjing University of Science and Technology, Nanjing, China, in 2006. He is currently a Professor at the Army Engineering University, Shijiazhuang, China. He has authored five book chapters, over 100 papers in journals and conferences, and holds one patents. His current research interests include automatic test system (ATS), network for equipment support, and analog to information conversion.

Cheng WANG was born in 1981, he received the Ph.D. degree from the Ordnance Engineering College, Shijiazhuang, China, in 2006. He is currently a Lecturer at the Army Engineering University. He has authored over 50 papers in journals and conferences, and holds one patents. His research interests include automatic test system (ATS), analog to information conversion, and intelligent signal processing.

Qiang WANG was born in 1992, he received the M.S. degree from the Army Engineering University, Shijiazhuang Campus, Shijiazhuang, China, in 2017, and received the M.S. degree from the Army Engineering University, Shijiazhuang Campus, Shijiazhuang, China, in 2021. His current research interests include compressive sensing and analog to information conversion.